Interannual Variability of OLR as Observed by AIRS and CERES

Joel Susskind, NASA Goddard Space Flight Center[1]
Gyula Molnar, Morgan State University/GESTAR[2]
Lena Iredell, Science Applications International Corporation[3]
Norman G. Loeb, NASA Langley Research Center[4]

[1]J. Susskind, NASA GSFC, Code 610, Greenbelt, MD 20771, Joel.Susskind@nasa.gov,
[2]G. Molnar, MSU/GESTAR, NASA GSFC, Code 610, Greenbelt, MD 20771, Gyula.I.Molnar@nasa.gov,
[3]L. Iredell, SAIC, NASA GSFC, Code 610, Greenbelt, MD 20771, Lena.Iredell@nasa.gov,
[4]N. Loeb, NASA LARC, Mail Stop 420, Hampton, VA 23681, Norman.G.Loeb@nasa.gov

Abstract

This paper compares spatial anomaly time series of OLR (Outgoing Longwave Radiation) and OLR_{CLR} (Clear Sky OLR) as determined using observations from CERES Terra and AIRS over the time period September 2002 through June 2011. Both AIRS and CERES show a significant decrease in global mean and tropical mean OLR over this time period. We find excellent agreement of the anomaly time-series of the two OLR data sets in almost every detail, down to the 1° x 1° spatial grid point level. The extremely close agreement of OLR anomaly time series derived from observations by two different instruments implies that both sets of results must be highly stable. This agreement also validates to some extent the anomaly time series of the AIRS derived products used in the computation of the AIRS OLR product. The paper also examines the correlations of anomaly time series of AIRS and CERES OLR, on different spatial scales, as well as those of other AIRS derived products, with that of the NOAA Sea Surface Temperature (SST) product averaged over the NOAA Niño-4 spatial region. We refer to these SST anomalies as the El Niño Index. Large spatially coherent positive and negative correlations of OLR anomaly time series with that of the El Niño Index are found in different spatial regions. Anomalies of global mean, and especially tropical mean, OLR are highly positively correlated with the El Niño Index. These correlations explain that the recent global and tropical mean decreases in OLR over the period September 2002 through June 2011, as observed by both AIRS and CERES, are primarily the result of a transition from an El Niño condition at the beginning of the data record to La Niña conditions toward the end of the data period. We show that the close correlation of global mean, and especially tropical mean, OLR anomalies with the El

Niño Index can be well accounted for by temporal changes of OLR within two spatial regions which lie outside the NOAA Niño-4 region, in which anomalies of cloud cover and mid-tropospheric water vapor are both highly negatively correlated with the El Niño Index. Agreement of the AIRS and CERES OLR_{CLR} anomaly time series is less good, which may be a result of the large sampling differences in the ensemble of cases included in each OLR_{CLR} data set.

1. Introduction

OLR (Outgoing Longwave Radiation) is a critical component of the Earth's radiation budget and represents the total radiation going to space emitted by the earth-atmosphere system and integrated over all angles. OLR products have been generated and monitored globally since 1975 based on broad spectral band measurements taken at a given satellite zenith angle by the ERB instrument on the Nimbus-6 and Nimbus-7 satellites (Jacobowitz et al. 1984, Kyle et al. 1993); the ERBE instrument on NOAA-9 and NOAA-10; ERBS (Barkstrom 1989); the AVHRR instrument on NOAA operational satellites (Gruber et al. 1994 and references therein); and most recently by CERES which has flown on EOS Terra since 2000 and on EOS Aqua since 2002 (Wielicki et al. 1996). Multiyear OLR data sets have also been generated via radiative transfer calculations, which compute OLR for a given scene using surface, atmospheric, and cloud products for that scene derived from the atmospheric sounders TOVS (Susskind et al. 1993) and AIRS (Susskind et al. 2011a).

OLR has been widely used as a proxy for tropical convective activity and rainfall, particularly in diagnosing and understanding tropical intraseasonal to interannual variability and monsoons (e.g., Kidson et al. 2002, Jones et al. 2004, Barlow et al. 2005,

Kiladis et al. 2005, Hoyos and Webster 2007, Wong et al. 2008, Chiodi and Harrison 2010, Loeb et al. 2012a). In addition, OLR has been used in studies of earth's radiation balance (e.g., Clement and Soden, 2005, Fasullo and Trenberth, 2008) and atmospheric model validation (e.g., Allan et al. 2003). More importantly, anomalies and trends of OLR have been used to study climate feedbacks and processes (e.g., Chu and Wang, 1997, Soden and Held 2006, Soden et al. 2008, Dessler et al. 2008, Huang and Ramaswamy 2009,Chung et al. 2010, Dessler 2010, Trenberth et al. 2010).

This paper has two main objectives. The first objective is to compare anomaly time-series of CERES and AIRS OLR products, generated by the CERES and AIRS Science Teams respectively, over the eight year 10 month overlap period of the two data sets, September 2002 through June 2011. This comparison shows excellent agreement of these anomaly time series down to the 1˚x 1˚ spatial scale. Behavior of OLR over this short time period should not be taken in any way as being indicative of what long term trends might be. The ability to begin to draw potential conclusions as to whether there are long term drifts with regard to the earth's OLR, or any geophysical parameter for that matter, would require consistent global observations for a time period of at least 20 years, if not longer. Nevertheless, a very close agreement of eight year 10 month OLR anomaly time series derived using two different instruments in two very different manners is an encouraging result. It demonstrates that one can have confidence in the eight year 10 month 1˚ x 1˚ OLR anomaly time series as observed by each instrument. The second objective of the paper is to explain why global mean, and especially tropical mean, OLR have decreased over the time period under study in

terms of the correlations between OLR anomaly time series on different spatial scales with the El Niño Index as defined later in this paper.

2. AIRS and CERES OLR data sets used

In this paper we use the operational monthly mean OLR and OLR_{CLR} data products produced by the AIRS and CERES Science Teams. We obtained the AIRS OLR products from the Goddard DISC and the CERES products from the CERES Science Team website. AIRS was launched on the EOS Aqua satellite in a 1:30 AM/PM local crossing time orbit in May 2002. The operational processing of AIRS data began after AIRS became stable in September 2002. We use the AIRS Version-5 monthly mean Level-3 1˚ x 1˚ latitude-longitude grid products which contain separate products generated for each of the 1:30 AM and PM local time orbits. We averaged the AM and PM products together to generate and use a single monthly mean product on the 1˚ x 1˚ grid for each month. In addition to AIRS OLR and OLR_{CLR}, we also use the AIRS Level-3 surface skin temperatures, water vapor profiles, and cloud products to demonstrate the behavior of factors contributing significantly to the anomaly time series of OLR and OLR_{CLR}. Section 3 provides a discussion of how the AIRS Science Team OLR and OLR_{CLR} products were computed at the Goddard DISC.

CERES has flown on both EOS Terra, which was launched in December 1999 on a 10:30 AM/PM local crossing time orbit, and on EOS Aqua, the same platform that carries AIRS. The CERES Science Team generates a number of different OLR data sets using CERES observations. The latest versions of the longest record CERES OLR data sets are referred to as the CERES EBAF (Energy Balanced And Filled) Edition-2.6r data sets, which like AIRS, are Level-3 products presented on a 1˚ x 1˚ latitude-

longitude grid. The CERES EBAF data set was obtained from http://ceres.larc.nasa/gov/order_data.php. CERES EBAF Edition-2.6r uses the latest calibration improvements with Edition-2 CERES cloud retrievals (Minnis et al. 2008, Minnis et al. 2011), angular dependence models (Loeb et al. 2005), and time-space averaging (Doelling et al. 2012). At the time of this writing, the Level-3 CERES Terra EBAF Edition-2.6r OLR data set extended to June 2011 and the AIRS Level-3 products extended to March 2012. There was no comparable EBAF Edition-2.6 data set available for CERES Aqua. For these reasons, the comparisons shown in this paper use CERES Terra and AIRS OLR products for the overlap time period September 2002 through June 2011.

3. Computation of AIRS OLR as a function of surface and atmospheric conditions

OLR at a given location is affected primarily by the earth's skin surface temperature, T_{skin}; skin surface spectral emissivity, ϵ_ν; atmospheric vertical temperature profile, T(p) and water vapor profile, q(p); and the heights, amounts, and spectral emissivities of multiple layers of cloud cover. OLR also depends on the vertical distributions of trace gases such as O_3(p), CH_4(p), CO_2(p), and CO(p). OLR is computed for a specific Field of Regard (FOR), given all the needed geophysical parameters, using an OLR Radiative Transfer Algorithm (RTA). Mehta and Susskind developed such an OLR RTA used in conjunction with the TOVS (TIROS Operational Vertical Sounder) retrieval methodology (Susskind et al. 1997) in order to generate the TOVS Pathfinder Path-A OLR data set (Mehta and Susskind 1999a, 1999b). AIRS OLR is computed using AIRS/AMSU sounding products in a completely analogous manner, including use of the same Mehta and Susskind OLR RTA (Susskind et al. 2003).

AIRS measures IR channel radiances over the interval 650 cm^{-1} to 2668 cm^{-1}. Most AIRS results shown in this paper were derived using the AIRS Science Team Version-5 retrieval algorithm (Susskind et al. 2011a) which generates the values of T_{skin}, ϵ_ν, T(p), q(p), O_3(p), and cloud parameters, from which OLR and OLR_{CLR} are computed. These geophysical parameters are determined for each AIRS 45 km x 45 km FOR which lies within a single AMSU-A footprint. The AIRS Version-5 OLR product, referred to as F below, is computed as a sum of fluxes in 14 contiguous spectral bands according to

$$F = \sum_{j=1}^{14} F_j = \sum_{j=1}^{14} \left(1 - \alpha\varepsilon_{1j} - \alpha\varepsilon_{2j}\right) F_{j,CLR} + \alpha\varepsilon_{1j} F_{j,CLD1} + \alpha\varepsilon_{2j} F_{j,CLD2} \qquad (1)$$

where $F_{j,CLR}$ is the computed clear sky flux going to space integrated over all angles emanating from spectral band j; $F_{j,CLDk}$ is the analogous computed flux emanating from an opaque cloud at cloud top pressure p_k; and $\alpha\varepsilon_{kj}$ is the radiatively effective cloud fraction where $\alpha\varepsilon_{kj}$ is the product of the geometric fractional cloud cover α_k as seen from above for the cloud at pressure p_k and the emissivity of that cloud in spectral band *j*.

Mehta and Susskind (1999a,b) parameterize F_j for a given sounding as a function of T_{skin}, surface spectral emissivity ε_j in spectral band *j,* T(p), q(p), and O_3(p). The parameterization coefficients used by Mehta and Susskind are computed based on line-by-line calculations (Susskind and Searl, 1978) which used the atmospheric line parameter data base of McClatchey et al. (1972). The spectral bands used in Equation 1 range from 2 cm^{-1} through 2750 cm^{-1}. There is no need to make radiometric measurements at all frequencies in order to perform the calculation shown in Equation 1. The AIRS Version-5 retrieval algorithm determines the surface spectral emissivity ε_ν

as a function of frequency over the AIRS spectral range using AIRS observations. Surface emissivities at frequencies lower than 650 cm^{-1} are set equal to those at 650 cm^{-1} and are irrelevant with regard to the computation of OLR in any event because the atmosphere is opaque at those frequencies. The AIRS Version-5 retrieval algorithm determines the effective cloud fraction $\alpha\varepsilon_{kj}$ at 800 cm^{-1} for each of up to two cloud layers k. The clouds are assumed to be gray, that is, $\alpha\varepsilon_k$ is assumed to be independent of frequency in the calculation of OLR. This is a valid approximation for opaque clouds but not so for cirrus clouds which have a cloud spectral emissivity which depends on the cloud drop size distribution. The results shown later in this paper demonstrates that the gray cloud approximation does not appear to have significant negative consequences with regard to the study of OLR anomaly time-series. No other approximations are made in the calculation of Equation 1.

AIRS OLR_{CLR}, the clear sky OLR, is also a product computed for each AIRS FOR obtained using Equation 1 but setting both $\alpha\varepsilon_1$ and $\alpha\varepsilon_2$ equal to zero. Geophysical parameters are determined from AIRS observations under both cloud-free and cloudy conditions, though their quality is poorer under very cloudy conditions, especially at or near the surface. For this reason, the AIRS Version-5 OLR_{CLR} product for a given FOR is included in the generation of the Level-3 monthly mean gridded OLR_{CLR} product only for those cases in which the AIRS retrieved cloud fraction is less than 90% and which also pass an OLR_{CLR} quality control procedure which indicates the retrieval is of acceptable accuracy down to the surface (Susskind et al. 2011a). Quality Controlled AIRS Version-5 OLR_{CLR} products that are included in the OLR_{CLR} Level-3 product are produced in roughly 75% of the FOR's observed by AIRS. The OLR product generated

for each FOR is always included in the Level-3 OLR product, both because of the need for complete sampling with regard to OLR, and also because computed values of OLR are not affected significantly by surface and atmospheric conditions beneath the cloud in very cloudy cases.

The CERES Science Team uses a different procedure for determining the ensemble of cases to be included in its Level-3 OLR_{CLR} product. The gridded CERES OLR_{CLR} product is generating by averaging values of CERES OLR only for those CERES footprints determined to be cloud-free by use of coincident MODIS spectral radiance measurements. The MODIS cloud mask used by the CERES Science Team is described in Minnis et al. (2011). As a result of this difference in sampling methodologies, the AIRS monthly mean OLR_{CLR} product includes a significantly larger ensemble of cases than that found in the CERES monthly mean OLR_{CLR} product. The significant sampling differences between the two ensembles of cases included in each OLR_{CLR} data set is most likely the largest factor that would negatively affect the comparison of OLR_{CLR} anomaly time series contained in the AIRS and CERES Level-3 data sets.

This paper also shows some results comparing OLR computed using the prototype AIRS Version-6 Science Team retrieval algorithm with the Version-5 OLR product. AIRS Version-6 uses an improved OLR RTA (Iacono et al. 2008) in the computation of OLR. The approach used to compute OLR in Version-6 is very similar to that used in Version-5, with the minor difference that 16 spectral bands are used in the computation of OLR as opposed to the 14 bands used in Equation 1. This new RTA does have two very important upgrades compared to Mehta and Susskind (1999a,b)

however. Most significantly, the new OLR RTA is generated using more up to date line absorption parameters, especially in the very strong water vapor absorption band near 300 cm^{-1}. In addition, the new OLR calculation allows for inclusion of the effects of variations in space and time of CO_2 profiles, as well as those of other minor absorption species such as CO, CH_4, and N_2O, in the calculation of OLR. The Version-5 OLR RTA did not include these effects and parameterized atmospheric transmittances only in terms of variable atmospheric profiles of temperature, water vapor, and ozone. The AIRS Version-6 retrieval algorithm also has other improvements in methodology which lead to improved values of the geophysical parameters themselves (Susskind et al. 2011b). The AIRS Science Team Version-6 retrieval algorithm is expected to become operational at the Goddard DISC in mid-2012. We obtained the Version-6 OLR results shown in the paper from the AIRS Science Team Computing facility at JPL. They are not available to the public at the time of the writing of this paper.

4. Comparison of AIRS and CERES OLR and OLR_{CLR} Data Records

Figure 1a shows global mean monthly mean values of AIRS Version-5 OLR and OLR_{CLR}, as well as those of CERES Terra EBAF Edition 2.6r OLR and OLR_{CLR}, henceforth referred to as CERES OLR and OLR_{CLR}, for the overlap period starting September 2002 and extending until June 2011. AIRS OLR and OLR_{CLR} products for parts of November 2003 and January 2010 were missing from the daily AIRS data record, and therefore observations for these days were not included in the generation at the DISC of the monthly mean OLR and OLR_{CLR} values for these months. We approximated what AIRS monthly mean OLR products for these months would have been if the whole month were observed, on a grid box basis, by setting grid point

differences between AIRS and CERES OLR for an incomplete month equal to the average value of the corresponding AIRS/CERES differences for the previous month and subsequent month, and adding these differences to the CERES monthly mean products. We used the same procedure to correct the AIRS OLR_{CLR} data records for those two months. We use these approximated OLR and OLR_{CLR} monthly mean records as if they were actual observations in the subsequent discussion.

Some reported monthly mean CERES OLR_{CLR} data points for individual 1 x 1° grid boxes have also been modified because these CERES OLR_{CLR} data values appeared to be significant outliers when compared to nearby CERES OLR_{CLR} values, as well as with colocated AIRS OLR_{CLR} values. For each grid box for each month, we eliminated any CERES OLR_{CLR} value that differed by more than 20 W/m^2 from the corresponding AIRS OLR_{CLR} value. We then spatially interpolated the remaining nearest values of the difference, CERES OLR_{CLR} minus AIRS OLR_{CLR}, to generate replacement values of this difference for the grid boxes that were found to be of questionable accuracy as described above. Note that only 2.6% of the CERES OLR_{CLR} monthly mean gridded values, which occurred primarily in the vicinity of Antarctica, were replaced in this manner. These replaced differences were then added to the AIRS OLR_{CLR} product for the corresponding grid boxes to generate the replacement values of CERES OLR_{CLR} which are used in all subsequent calculations.

We observe a number of features in Figure 1a. The most prominent result is that to first order, the AIRS and CERES OLR and OLR_{CLR} data sets appear to be biased compared to each other. Figure 1b presents the differences between the AIRS and CERES monthly mean global mean values of OLR and OLR_{CLR} shown in Figure 1a. The

difference between AIRS Version-5 OLR and CERES OLR shows a small annual cycle superimposed on a nearly constant bias. Part of this annual cycle, with a maximum in June and a minimum in December, may be the result of the large diurnal cycle of OLR over land. The CERES Science Team adjusts for the effects of the diurnal cycle on CERES Terra observations as described in Loeb et al., 2012b (supplementary information). The AIRS monthly mean OLR product averages daytime and nighttime OLR observations together but does not make any other correction for diurnal cycle. Figure 1b also contains horizontal lines showing the average value of each difference. The average value of the difference between AIRS and CERES OLR, computed over the eight year time period September 2002 through August 2010, is 8.62 W/m^2. This average difference was computed over a full eight year period so as to minimize the effect of the annual cycle on its value.

The differences between AIRS and CERES OLR_{CLR} are similar to, but smaller than, those of OLR, with regard to both their mean value and their seasonal cycle. The mean value of AIRS minus CERES Terra OLR_{CLR} is 8.03 W/m^2, which is roughly 0.6 W/m^2 less than that of AIRS minus CERES Terra OLR. The seasonal cycles of the differences between AIRS and CERES OLR on the one hand, and AIRS and CERES OLR_{CLR} on the other, are displaced in time relative to each other. This displacement might be a result of the significant sampling differences in the cases included in the AIRS and CERES OLR_{CLR} data sets, respectively.

The large biases between the AIRS Version-5 OLR and OLR_{CLR} data records and those of CERES are at first disconcerting but are readily understood. The AIRS OLR product derived using the AIRS Science Team Version-6 retrieval algorithm has

been found to have much smaller biases compared to CERES Terra OLR than does AIRS Version-5 OLR. The substantial, though nearly constant in time bias between OLR as computed from AIRS products and observed by CERES is primarily a result of the use of an older set of line by line absorption coefficients in the parameterization of the Version-5 OLR RTA (Mehta and Susskind 1999a,b), compared to that used in the improved OLR RTA (Iacono et al. 2008) used in Version-6. The main difference between the two OLR parameterizations is that the Iacono et al. (2008) OLR RTA has more absorption in the water vapor rotational band near 300 cm^{-1} than does Mehta and Susskind (1999a). As a result of this, lower values of OLR would be computed in Version-6, compared to those computed in Version-5, especially under very moist conditions. Globally, there is more water vapor in the atmosphere in the northern hemisphere summer, and less in the northern hemisphere winter, than in the annual mean. This would contribute to the larger (more positive) differences in the Version-5 OLR product from that of CERES OLR product in the northern hemisphere summer, and smaller (less positive) OLR differences in the northern hemisphere winter, as shown in Figure 1b.

A prototype of the AIRS Version-6 retrieval algorithm has been run at the AIRS Science Team Facility for April 2003 and April 2011. Monthly mean values of AIRS Version-6 OLR and OLR_{CLR} for these months are indicated in Figure 1a by blue triangles and blue squares respectively. Figure 1b includes the monthly mean differences between AIRS Version-6 OLR and CERES OLR for these months, shown in green triangles, with values of 3.24 W/m^2 and 3.27 W/m^2 for April 2003 and April 2011, respectively, and the differences between AIRS Version-6 OLR_{CLR} and CERES OLR_{CLR},

shown in red squares, with values of 0.67 W/m^2 and 0.70 W/m^2. It is therefore expected that AIRS Version-6 OLR and OLR_{CLR} time series will be significantly closer to those of CERES Edition 2.6 than the corresponding time series of AIRS Version-5, at least in the mean sense. The remainder of this paper will include a comparison of anomaly time series of AIRS Version-5 OLR and OLR_{CLR} with those obtained from CERES. Anomaly time-series obtained from two different sets of instruments can agree very well with each other even if the individual data sets are biased against each other, provided the bias for a given month of the year is essentially constant in time.

5. Comparison of AIRS and CERES Global Mean and Tropical Mean Anomaly Time Series

We generated AIRS and CERES monthly mean OLR and OLR_{CLR} climatologies on a 1° x 1° spatial resolution for each month of the year by taking the average of the grid box value for that month over an eight-year time period, i.e., eight consecutive Januaries, eight consecutive Februaries, etc. The same ensembles of eight Januaries, Februaries, etc., are used in the generation of climatologies for all products shown in this paper. OLR and OLR_{CLR} anomalies for a given month in a given year, on a 1° x 1° spatial grid, are defined as the differences between their monthly mean values in that year and their monthly climatologies for that grid box. The area mean anomaly for a given month is defined as the cosine latitude weighted average of the grid box anomalies contained in the area under consideration.

Figure 2a shows the global mean anomaly time series of AIRS Version-5 OLR and CERES OLR for the period September 2002 through June 2011, as well as the difference between the two sets of monthly mean anomalies. Figure 2b shows

analogous results for tropical mean OLR anomalies, and Figures 2c and 2d show analogous global mean and tropical mean anomaly time series for the AIRS and CERES OLR_{CLR} products. We define a term, the El Niño Index, as the difference of the NOAA monthly mean oceanic Sea Surface Temperature (SST), averaged over the NOAA Niño-4 spatial area 5˚N to 5˚S latitude and 150˚W westward to 160˚E longitude, from a NOAA Niño-4 SST monthly mean climatology we generated in an analogous manner to that used in the generation of the OLR climatologies. Figures 2b and 2d include the values of the El Niño Index multiplied by 1.5. All anomaly time-series shown in Figures 2a-2d, as well as anomaly time series shown in subsequent figures, have a three point smoother applied to them.

Tropical mean OLR and OLR_{CLR} anomalies both tend to track those of the El Niño Index in phase fairly closely, but the greatest tropical mean OLR anomalies are almost twice as large as the greatest OLR_{CLR} anomalies. Positive values of the El Niño Index (2003, 2005, 2007, early 2010) correspond to El Niño (positive SST anomalies in the Niño-4 area) periods, and negative values (2008, mid-2010 to the present) correspond to La Niña (negative SST anomalies) periods. Figures 2a and 2c show that an onset of negative global mean anomalies for both OLR and OLR_{CLR} began in late 2007. The negative tropical mean anomalies of both OLR and OLR_{CLR} shown in Figures 2b and 2d are generally considerably larger than the corresponding global mean anomalies, especially after mid-2007. The decreases in global mean OLR and OLR_{CLR} in late 2007 are strongly influenced by the significant reduction in tropical mean OLR and OLR_{CLR} which started a few months earlier. Tropical mean OLR and OLR_{CLR} anomalies became positive starting in late 2009, roughly coincident with the onset of another El Niño event.

Very substantial negative global and especially tropical mean OLR anomalies occurred in the period starting mid-2010, when the latest La Niña event began. Loeb et al. (2012a, 2012b)) has already pointed out the existence of this relationship between CERES OLR anomalies and El Niño/La Niña activity.

The difference between AIRS and CERES tropical mean OLR anomaly time series, shown in green in Figure 2b, is positively correlated with the El Niño Index, with a temporal correlation of 0.52. This is a result of fact that both positive and negative tropical mean AIRS OLR anomalies are slightly larger in magnitude than those of CERES. An analogous result is found with regard to the difference between AIRS and CERES global mean OLR, which has a temporal correlation of 0.51 with the El Niño Index.

5.1 Average Rates of Change and El Niño Corrrelations of Anomaly Time Series

We define the Average Rate of Change (ARC) of an anomaly time series as the slope of the linear least squares fit of the anomaly time series. We use the term Average Rate of Change to describe the slope of an anomaly time series rather than the term Trend, which is generally used to characterize long-term multi-decadal data sets rather than the eight year 10 month period studied in this paper. Figure 2b shows that the El Niño Index is highly non-linear over this time period, with fluctuating values that are primarily positive at the start of the time period and substantially negative at the end of the time period. The ARC of the El Niño index, computed over the time period September 2002 through June 2011, is -0.123 ± 0.046K/yr. The uncertainties shown here and subsequently represent twice the standard error, σ, of the regression slope of the linear least squares fit (Draper and Smith, 1981). The precise value of the ARC of

the El Niño index, which depends on the length of the time period used in the calculation, is less important than its sign, which shows that the El Niño region has cooled on the average over the time period under study.

Spatial distributions of ARCs of OLR and other geophysical parameters will be shown later in the paper. Spatial distributions of ARCs of geophysical parameters are very coherent and are particularly informative with regard to the understanding of why global mean and tropical mean OLR have decreased over the period September 2002 through June 2011. In this context, it is also very informative, if not more so, to examine the spatial distribution of temporal correlations of 1° x 1° grid point anomaly time series with that of the El Niño index. We refer to these temporal correlations of anomaly time series around the earth with the single anomaly time series of T_{skin} averaged over the NOAA Niño-4 region as El Niño Correlations (ENCs). ENCs represent both the phase and magnitude of the relationship between the time series of grid point anomalies and that of the El Niño Index. Unlike ARCs, ENCs should not depend significantly on the extent of the time series used to compute them if these correlations hold up over long time periods. There should be a very close agreement between the spatial patterns of ARCs of OLR with those of the ENCs of OLR in those spatial areas in which the ARCs of OLR are strongly influenced by El Niño/La Niño activity, and these patterns will be of opposite sign as a result of the negative ARC of the El Niño Index.

Table 1a shows global mean and tropical mean values of the ARCs of AIRS OLR and CERES Terra OLR anomalies over the time period September 2002 through June 2011, the standard deviations between the two sets of global mean and tropical mean anomaly time series, and the temporal correlations between each global mean and

each tropical mean anomaly time series. All statistics use values of the three point smoothed anomaly time series shown in Figure 2. The agreement of the ARCs of both global mean and tropical mean anomaly time series found in the AIRS and CERES OLR records is on the order of ±0.03 W/m^2/yr, which is within the uncertainty of the respective sets of ARCs. The temporal correlations of the AIRS and CERES global mean and tropical mean OLR anomaly time series are 0.955 and 0.991 respectively. Both AIRS and CERES OLR anomaly time series show that global mean OLR has decreased on the average on the order of -0.075 W/m^2/yr over the time period September 2002 through June 2011, and that tropical mean OLR has decreased at a rate of roughly -0.168 W/m^2/yr from the beginning of the time period to the end. Demonstration of the ability to obtain close agreement between global and tropical mean ARCs of AIRS and CERES OLR anomaly time series, obtained in very different manners, is more significant than the values of the ARCs themselves, which are influenced by the extent of the time period used in the AIRS/CERES OLR data record comparison.

Table 1b shows analogous statistics comparing AIRS and CERES OLR_{CLR} anomaly time series. The correlations between the AIRS and CERES OLR_{CLR} anomaly time series are still high, but somewhat reduced from those of the OLR anomaly time series. In addition, the standard deviations of the OLR_{CLR} anomaly differences are also somewhat larger than those of OLR, and the global and tropical mean ARCs of OLR_{CLR} found in both data sets, while still negative, do not agree as closely as those of OLR. Nevertheless, the agreement obtained between anomaly time series of AIRS and

CERES OLR_{CLR} is better than might be expected given the significant sampling differences between the cases included in each monthly mean OLR_{CLR} data set.

Table 1c shows temporal correlations between global mean and tropical mean anomaly time series of OLR and OLR_{CLR} as well as the correlations (ENCs) of the anomaly time series with the El Niño Index. Correlations using AIRS time series are shown above the diagonal in bold and those using CERES time series are shown beneath the diagonal. As shown in Table 1c, the temporal correlation between the CERES global and tropical mean OLR anomaly time series is 0.646, and the corresponding correlation for the AIRS anomaly time series is 0.705. This shows that tropical anomalies provide a significant contribution to the global OLR anomaly time series found in both data sets. The CERES and AIRS tropical mean OLR anomaly time series also correlate very highly with the El Niño index, with correlations greater than 0.8. CERES and AIRS tropical mean OLR_{CLR} anomaly time series also have high correlations with the El Niño Index, though somewhat smaller than those of the corresponding OLR data sets. Both sets of global OLR and OLR_{CLR} anomaly time series also show moderate correlations, on the order of 0.55, with the El Niño Index. These correlations of global and tropical anomaly time series with the El Niño Index further imply that the recent short term decreases in global and tropical OLR over the time period September 2002 through June 2011, as observed by both AIRS and CERES, are strongly influenced by changes from El Niño conditions at the beginning of the time series to La Niña conditions at the end.

5.2 The Spatial Distribution of ARCs and ENCs of OLR

This section compares the spatial distribution of ARCs of AIRS and CERES OLR

with each other on a 1˚ latitude by 1˚ longitude basis, as well as the spatial distribution of the correlations of the anomaly time series with the El Niño Index (ENCs). These comparisons not only show excellent agreement of ARCs and ENCs of AIRS OLR products with those of CERES on a small spatial scale, but also depict the spatial regions that have been contributing significantly to the short term decreases in global mean and tropical mean values of OLR over the period under study.

The global spatial distributions of OLR ARCs over the time period September 2002 through June 2011 are shown in Figures 3a and 3b for AIRS and CERES, respectively. As discussed previously, more significant than the values of the ARCs shown in Figure 3 is the very coherent spatial structure of the ARCs of OLR. Figures 3a and 3b demonstrate two very important points. The first is the virtually indistinguishable spatial distributions of the ARCs of AIRS OLR and of CERES OLR. Figure 3c shows their difference, with a spatial correlation of 0.98 between the ARCs of the 2 OLR data sets, and a standard deviation of 0.15 $W/m^2/yr$. The global mean AIRS OLR ARC for this period is 0.035 $W/m^2/yr$ lower (more negative) than that of CERES Terra. This small difference is not monolithic, but occurs primarily near 30°S latitude, especially over Eastern Australia in which the large negative ARCs of OLR are greater in AIRS than in CERES.

The most important point of Figures 3a and 3b is that while the global mean and tropical mean ARCs of OLR are negative, there is considerable spatially coherent longitudinal structure of the ARCs of OLR at a given latitude, with differing signs and amplitudes. This structure is largest in the tropics, but is found at other latitudes as well. Figure 3 shows that positive OLR ARCs as large as 4.2 $W/m^2/yr$ exist in the vicinity of

the equatorial dateline. These are more than compensated for, in the tropical mean sense, by negative OLR ARCs at other longitudes, as large as − 3.2 W/m^2/yr near the equator over Indonesia in the vicinity of 120°E longitude.

Figures 3a-d, and some subsequent figures, contain boxes surrounding three areas. A box, shown in gray, surrounds the NOAA Niño-4 region, 5°N to 5°S and 150°W westward to 160°E. A second box, shown in black, covers portions of the Eastern tropical Pacific Ocean, Northern South America, and the equatorial Atlantic Ocean and is the composite of three adjacent rectangles: 5°N to 20°S, 140°W to 95°W; 8°N to 20°S, 95°W to 70°W; and 8°N to 8°S, 70°W to 10°E. We will refer to the area encompassed by these three contiguous rectangles as OLR Region 1. A third box, also shown in black, encompasses the area between 15°S to 30°S and 135°E eastward to 165°W. We will refer to the area encompassed by this box as OLR Region 2.

ARCs of OLR within OLR Region 1 and OLR Region 2 are very negative over the period September 2002 through June 2011. The decreases in OLR that took place in these two regions will be shown later in the paper to account for most of the decreases observed in global and tropical mean OLR which occurred during this time period. OLR Regions 1 and 2 were selected entirely based on the results shown in Figures 3a and 3b. These regions were chosen both so as to be composed of contiguous rectangular parts and also to encompass key features shown in these figures. OLR Region 2 is essentially in the “heart” of the area referred to as the South Pacific Convergence Zone, which varies its location according to the phases of the El Niño – Southern Oscillation (ENSO) and of the Interdecadal Pacific Oscillation (Folland et al. 2002, Brown et al. 2011).

The spatial distributions of the ARCs of AIRS and CERES OLR_{CLR} are not shown here, but the difference between the ARCs of the two OLR_{CLR} data sets is shown in Figure 3d. The general agreement is again reasonably good, with a spatial correlation of 0.82. Figure 3d shows that much of the positive difference of AIRS global mean ARCs of OLR_{CLR} compared to CERES occurs over the oceans between the latitudes 50°N and 60°S. We do not understand the causes of these differences in OLR_{CLR} at this time but they are most likely, at least in part, a result of the significant sampling differences of the ensembles of cases included in the AIRS and CERES monthly mean OLR_{CLR} products. The remainder of this paper will deal only with the OLR products.

Figures 4a-4c are analogous to Figures 3a-3c but show patterns of ENCs of AIRS and CERES OLR and their difference. As found with regard to ARCs of OLR, there is again considerable spatial structure, and excellent agreement, in the ENCs of AIRS and CERES OLR, with a global spatial correlation of 0.97. This agreement shows that not only are the slopes of high spatial resolution anomaly time series of AIRS and CERES OLR in close agreement, but implies that the anomaly time series themselves are also in close agreement.

The spatial structure of ENCs of OLR closely follows that of the OLR ARCs but with opposite sign, especially in the tropics. For example, the area of large positive ARCs of OLR including and surrounding the NOAA Niño-4 region has OLR anomalies which are highly negatively correlated with the El Niño Index, that is, periods of positive SST anomalies in the Niño-4 region correspond to negative OLR anomalies in this and surrounding areas. This anti-correlation of the spatial distributions of ARCs and ENCs of tropical OLR between September 2002 and June 2011 indicates that the tropical ARCs

of OLR shown in Figure 3 are very strongly influenced by time periods containing significant El Niño/La Niña activity. The origin of these patterns will be addressed in more detail later in the paper when ENCs of mid-tropospheric water vapor and cloud cover are discussed.

The inverse relationship between spatial patterns of ARCs and ENCs holds in some extra-tropical areas as well. Globally, the spatial distribution of ARCs and ENCs of OLR have correlations of -0.78 and -0.79 for AIRS and CERES respectively. It is interesting to note that differences between ARCs of AIRS and CERES OLR (Fig. 3c) are also anti-correlated with the differences in their ENCs (Fig. 4c), with AIRS tropical OLR anomaly correlations with El Niño activity being slightly higher than CERES OLR anomaly correlations, thus resulting in slightly more negative tropical ARCs of AIRS OLR compared to CERES as shown in Table 1a.

Figures 4a and 4b are very similar in appearance, but with opposite sign, to Figure 3 of Davies and Molloy (2012), which shows the spatial distribution of the temporal correlation of cloud top height anomalies H′ derived from MISR with the Southern Oscillation Index over the period 2000 through 2010. The sign reversal is expected because OLR decreases with increasing H′, and the Southern Oscillation Index is similar to, and in phase with, the El Niño Index.

The spatial correlations of the anomaly time series of AIRS OLR with those of CERES OLR for each 1° by 1° grid point are shown in Figure 4d. The global mean AIRS/CERES OLR anomaly time series correlation, on a 1° x 1° spatial scale, is 0.93, with the largest differences occurring in the mid-latitudes and over convective areas in South American and Africa. This shows that as with their ARCs and ENCs, AIRS and

CERES OLR anomaly time series on a 1° x 1° spatial scale also agree closely with each other.

5.3. Longitudinal Distribution of Equatorial Anomaly Time Series: Hovmöller Diagrams

Figures 3 and 4 show that the tropics contain large spatially coherent areas with alternating values of positive and negative ARCs and ENCs of OLR over the time period under study. This section compares CERES and AIRS Hovmöller diagrams of OLR, which show the longitudinal distribution of near equatorial anomaly time series of CERES and AIRS OLR.

Figure 5a and 5b present Hovmöller diagrams showing time series of monthly mean AIRS and CERES OLR anomalies (vertical scale), integrated over the latitude range 5°N through 5°S, in each 1° longitude bin (horizontal scale) for the time period September 2002 through June 2011. The difference between the AIRS OLR Hovmöller diagram and the CERES OLR Hovmöller diagram is shown in Figure 5c. Figures 5a and 5b, and all subsequent Hovmöller diagrams, have a small amount of smoothing applied to them. A five point (five month) smoothing was applied in the vertical and a 15 point (15 degree) smoothing was applied in the horizontal to minimize the effects of small discontinuities between adjacent rectangular grid points on the figures. Most of the region covered is ocean. There are three relatively small land areas near the equator: South America, Africa, and Indonesia. These land areas each lie between the three sets of narrow black vertical lines shown in Figure 5, one of which is covered by one of the two thick black vertical lines included in Figure 5. These lines at 140W and 10˚E,

encompass the longitudinal domain of OLR Region 1. The thick black line at 10°E lies on top of the thin line at the western edge of Africa.

The two sets of Hovmöller diagrams of tropical OLR anomalies are essentially identical, with a correlation coefficient of 0.995 between them. Some of the largest differences between the AIRS and CERES tropical anomaly time series occur in November 2003 and January 2010, the two months for which AIRS data was synthesized. The differences between AIRS and CERES in these two months would have been much larger if the AIRS "monthly mean" OLR products stored at the Goddard DISC were used in the calculations, as we did originally. In both cases, the AIRS "monthly mean" products of the DISC represented averages over less than a month time period, while the CERES data represented observations taken over the entire month. The fact that the remainder of the OLR anomaly differences shown in Figure 5c were so small alerted us to check, and correct for, the cause of the problem with these two months.

The anomaly time series shown in Figure 5 depict the phase relationship of OLR anomalies at different longitudes in the vicinity of the equator as a function of time. Such figures provide insight into the spatial distribution of tropical ARCs and ENCs of OLR in the vicinity of the equator shown in Figures 3 and 4. In the longitudinal band 160°W westward to 140°E, equatorial OLR anomalies were very negative in late 2002/early 2003 which corresponds to an El Niño period. The very positive OLR anomalies in this same longitudinal band from mid-2007 through early 2009 and mid-2010 through June 2011 both occur during La Niña periods. These features give rise to the substantial positive OLR ARC shown in Figures 3a and 3b over the region 5°N – 5°S, 160°W to

140˚E. Figure 3 shows very negative values of OLR ARCs near the equator between 100˚E and 140˚E longitudes. Figure 5 shows that equatorial OLR anomalies between 100˚E and 140˚E are out of phase with those between 140˚E and 160˚W and are of comparable magnitude. Figure 5 also shows that equatorial OLR anomalies from 140˚W eastward to 10˚E, within the longitudinal domain of OLR Region 1, tend to be smaller than, and out of phase with, those from 160˚W westward to 140˚E , especially during La Niña periods. This phenomenon gives rise to the negative equatorial OLR ARCs shown in Figure 3 contained within OLR Region 1. The phase relationships discussed above are also reflected in the ENCs of equatorial OLR shown in Figure 4.

6. The Effect of Phases of El Niño/La Niña on Tropical Water Vapor, Cloud Cover, and OLR Anomaly Time Series

Figures 3 to 5 show that the spatial patterns of both the Average Rates of Change and El Niño Correlations of OLR over the time period September 2002 through June 2011, as observed by AIRS and CERES, are in excellent agreement with each other, as are their equatorial anomaly time series in the vicinity of the equator. Both CERES and AIRS OLR products show that the period September 2002 through June 2011 is marked by a substantial decrease in global mean OLR, on the order of $-0.075\ W/m^2/yr$, and a larger decrease in tropical mean OLR on the order of $-0.165\ W/m^2/yr$. This agreement of Average Rates of Change of OLR anomaly time series derived from observations by two different instruments, in totally independent and different manners, implies that both sets of OLR products must be stable over the eight year 10 month period in which they were compared. There should be little question that there actually was a significant decrease of global mean OLR over the time period

September 2002 through June 2011, and that the majority of the decrease occurred in the tropics.

These results, found by both CERES and AIRS, should not be taken as indicative in any way as to what will happen in the future. It mainly shows that OLR anomalies and their Average Rates of Change can be determined very accurately by two totally independent instrumental and theoretical approaches. The agreement of anomaly time series of OLR as determined using CERES and AIRS observations also indirectly validates the anomaly time series of the AIRS derived products used in the computation of AIRS OLR, at least for the time period September 2002 through June 2011.

This section uses anomaly time series of AIRS derived products to explain the factors contributing to the anomaly time series of OLR over the period under study and why OLR anomalies are highly correlated with the El Niño Index. Figures 6a and 6b show the spatial distribution of the ARCs and ENCs of AIRS Version-5 T_{skin} over the period September 2002 through June 2011. The results shown in these figures provide important insight toward the understanding of the spatial distribution of ARCs and ENCs of OLR, as well as those of other related geophysical parameters on which OLR depends. Aside from T_{skin}, OLR also depends significantly on the atmospheric temperature profile T(p) and atmospheric water vapor profile q(p), and in the tropics, even more so on the cloud top pressure p_c and radiatively effective cloud fraction $\alpha\varepsilon$. It is impractical to show results relating to anomaly time series of all the important geophysical parameters affecting those of OLR. In this paper, for demonstrative purposes, we concentrate on 500 mb specific humidity q_{500} and radiatively effective cloud fraction $\alpha\varepsilon$. The OLR calculations of course take into account the detailed

changes in the entire water vapor profile and the heights and amounts of clouds, as well as those of the temperature and ozone profiles on which OLR also depends.

A number of important features are found in Figure 6a. While the global mean ARC of T_{skin} is essentially zero over this time period, there are areas in which significant positive and negative T_{skin} ARCs exist. There has been considerable warming near the North Pole over this time period, as well as considerable warming and cooling in different areas over Northern Hemisphere extra-tropical land. In addition, there has been substantial cooling over much of Africa, especially south of 15°S, as well as over much of Australia. All of these areas in which extra-tropical land has either warmed or cooled considerably over the time period under study are also characterized by increases or decreases in OLR as shown in Figure 3. This is consistent with the fact that everything else being equal, increases (decreases) in T_{skin} results in increases (decreases) in OLR.

Figure 6a also shows that the tropics are marked by a substantial oceanic surface temperature cooling over and immediately surrounding the Niño-4 region contained within the gray rectangle. This area of oceanic cooling over the last nine years is surrounded to the south, west, and north by areas in which oceanic warming occurred during this period, though to a lesser extent. Figure 3 shows that OLR changes in these oceanic areas are considerable, and unlike over extra-tropical land, are of opposite sign to those of the changes in T_{skin}. This indicates that the changes in tropical oceanic OLR in these regions are driven by changes in something other than T_{skin}.

Figure 6b shows that as in the case of OLR, ENCs of T_{skin} are generally of opposite sign to their ARCs. The global mean spatial correlation of ARCs and ENCs of T_{skin} is -0.56, which is still appreciable but smaller than that for OLR. It is apparent from Figures 6a and 6b that the considerable cooling of T_{skin} that took place over South Africa and Australia is related to a strong in phase response of T_{skin} to El Niño/La Niña activity in these areas. On the other hand, the significant changes in T_{skin} that occurred over Northern Hemisphere extra-tropical land, such as the warming that occurred near the North Pole, are not in direct response to El Niño activity because ENCs of T_{skin} in these areas are not appreciable. It is also interesting to note that in some equatorial oceanic areas, such as in the vicinity of 90°W and 60°E, T_{skin} anomalies had moderate positive correlations with El Niño activity but T_{skin} in those areas had very small Average Rates of Change. In addition, while ARCs and ENCs of OLR within OLR Region 1 were all large and of the same sign, this is not the case with regard to T_{skin}, in which ARCs and ENCs of T_{skin} are of opposite sign in the Atlantic Ocean portion of OLR Region 1 as compared to the Pacific Ocean. An analogous result occurs within OLR Region 2 in which ARCs and ENCs of T_{skin} are of opposite sign over Australia as compared to the Pacific Ocean to the East.

Figures 6c and 6d show ENCs of 500 mb specific humidity q_{500} and effective cloud fraction $\alpha\varepsilon$, respectively. In the tropics, ARCs of q_{500} and $\alpha\varepsilon$ (not shown) are out of phase with ENCs of these parameters, as was the case with ARCs and ENCs of OLR. OLR is very sensitive to the concentration of mid-upper tropospheric water vapor in very moist (i.e., most tropical) areas, in the sense that increasing water vapor concentration increases atmospheric absorption in some spectral bands and therefore lowers OLR,

everything else being equal. OLR also decreases with increasing cloud cover, especially for high clouds. As with T_{skin}, ENCs of q_{500} and $\alpha\varepsilon$ are both very positive in the Niño-4 region. This high positive correlation with El Niño activity resulted in both a significant overall mid-tropospheric drying and a corresponding overall decrease in cloud cover over the period under study in this region. An analogous situation occurs in the surrounding areas of warming surface skin temperature, in which ENCs of q_{500} and $\alpha\varepsilon$ are very negative, resulting in considerable mid-tropospheric moistening as well as increasing cloud cover in these regions during the period under study. Unlike T_{skin} however, there are also large negative ENCs of q_{500} and $\alpha\varepsilon$ contained within most of OLR Region 1 over this time period, resulting in both considerable mid-tropospheric moistening and increasing cloud cover over most of OLR Region 1. Again, unlike T_{skin}, on the average, OLR Region 2 also is marked by large negative ENCs of q_{500} and $\alpha\varepsilon$, indicating that there has been considerable mid-tropospheric moistening and increasing effective cloud fraction within most of OLR Region 2 over the time period under study as well.

As with OLR, Hovmöller diagrams provide a good depiction of the interrelationship of equatorial anomalies of different geophysical parameters as a function of time and longitude. The Hovmöller diagram of monthly mean AIRS T_{skin} anomalies for the period September 2002 through June 2011 is shown in Figure 7a. The vertical gray lines in Figure 7a delineate the longitudinal band containing the Niño-4 region, 150°W longitude westward to 160°E longitude. The largest T_{skin} anomalies tend to occur on either side of the dateline between these longitudinal limits. Figure 7a clearly demonstrates that the large negative T_{skin} ARC in the Niño-4 region shown in

Figure 6a is the result of the transition from an El Niño condition (locally positive T_{skin} anomaly) at the end of 2002 to La Niña conditions (locally negative T_{skin} anomalies) over the time periods late 2007 through 2008, and especially late 2010 through mid-2011. Equatorial T_{skin} anomalies between 100°E and 140°E tend to be smaller than, and of opposite sign to, those in the vicinity of the dateline. This gives rise to the band of weaker positive T_{skin} ARCs near the equator from 100°E to 140°E shown in Figure 6a. T_{skin} anomalies in the equatorial Atlantic Ocean are also to some extent out of phase with those in the Niño-4 region, resulting in the small positive ARCs, and moderately negative ENCs, of T_{skin} in the equatorial Atlantic Ocean as shown in Figures 6a and 6b.

Figure 7b and 7c show the Hovmöller diagrams of q_{500} and $\alpha\epsilon$. As in Figure 5, the vertical thick black lines delineate the longitudinal extent of OLR Region 1, extending from 140°W eastward to 10°E. Anomalies of q_{500} and $\alpha\epsilon$ near the dateline generally both follow those of T_{skin} very closely, both in magnitude and in phase. This indicates, not surprisingly, that positive SST anomalies in the Niño-4 region correspond to periods of increased convection in that area, leading to enhancement of moisture in the mid-troposphere as well as increases in cloud cover. Conversely, negative SST anomalies in the Niño-4 area correspond to periods of decreased convection (increased subsidence) leading to periods of a drier mid-troposphere and decreases in cloud cover. Water vapor and cloud cover anomalies over Indonesia, from roughly 100°E to 140°E, are out of phase with those near the dateline, as was found for T_{skin}. Unlike T_{skin} anomalies over Indonesia, which were smaller than those near the dateline, q_{500} and $\alpha\epsilon$ anomalies over Indonesia are closer in magnitude to those near the dateline. This is the result of the westward shift of the area of maximum convection during La Niña periods

from the dateline to Indonesia. This out-of-phase relationship gives rise to the very substantial negative ENCs of q_{500} and $\alpha\epsilon$ over Indonesia during this time period, as shown in Figures 6c and 6d.

Figures 6c and 6d contain substantial negative ENCs of q_{500} and $\alpha\varepsilon$ in some tropical locations in which no significant changes in T_{skin} exist. The most notable of these is off the west coast of South America, in the vicinity of 5°N to 20°S from 120°W eastward to 80° W, which is a part of OLR Region 1. There is also another region of positive q_{500} ENCs near the equator going across South America and extending eastward along the Atlantic Ocean to about °E longitude, which is also contained within OLR Region 1. Figures 7b and 7c show that equatorial water vapor and cloud cover anomalies off the west coast of South America are often out of phase with those at the dateline, especially during the large La Niña events in 2007-2008 and 2010-2011. This demonstrates that La Niña periods of decreased convection near the dateline also correspond to periods of increased convection eastward of 120°E, as a result of the eastward shift of the convective branch of the Walker circulation during La Niña periods (Power and Smith 2007; Zhou et al. 2011). The same relationship is found to a lesser extent over the Atlantic Ocean extending to E longit ude at the eastern end of OLR Region 1.

The Hovmöller diagrams of q_{500} and $\alpha\epsilon$, shown in Figures 7b and 7c, are very highly negatively correlated with that of OLR, shown in Figure 5. The Hovmöller diagrams of q_{500} and $\alpha\epsilon$ have correlations of -0.79 and -0.93 respectively with those of AIRS OLR, and -0.79 and -0.92 with those of CERES OLR. This further demonstrates

that anomalies in tropical mid-tropospheric water vapor, and especially in cloud cover, are the driving forces behind changes in tropical OLR.

7. Attribution of Recent Decreases in Global and Tropical Mean OLR to Changes Contained within OLR Regions 1 and 2

Figure 3 shows that the largest OLR ARCs occur in the tropics regions covering Indonesia and near the dateline. OLR ARCs in these areas are roughly equal to each other and of opposite sign, as are the OLR anomaly time series shown in Figure 5. The effects of the large positive and negative tropical OLR ARCs near the dateline and over Indonesia tend to cancel in the zonal mean sense. The large negative tropical mean ARC of OLR results primarily from OLR anomalies in OLR Region 1. These in turn are strongly influenced by water vapor and cloud cover anomalies in OLR Region 1, both of which are very negatively correlated with El Niño activity.

Table 2 shows values of ARCs and ENCs of OLR averaged over different spatial regions, as determined using each of the AIRS and CERES OLR data sets. ARCs of OLR anomalies averaged over OLR Region 1, and especially over OLR Region 2, are considerably larger than the corresponding tropical mean ARCs shown in Table 1a. On the other hand, the ENCs of AIRS and CERES OLR in OLR Regions 1 and 2 are comparable to each other, as well as to the corresponding tropical mean OLR ENCs shown in Table 1c.

The negative tropical mean OLR ARC over the period September 2002 through June 2011 computed as previously, but after replacing OLR ARCs in OLR Region 1 by zeroes, is reduced from -0.183 W/m^2/yr to -0.037 W/m^2/yr for AIRS, and from -0.154 W/m^2/yr to -0.011 W/m^2/yr for CERES. Likewise, the negative global mean AIRS OLR

ARC, excluding ARCs within Region 1, is reduced from -0.094 W/m^2/yr to -0.044 W/m^2/yr, and from -0.059 W/m^2/yr to -0.011 W/m^2/yr for CERES. This indicates that both OLR data sets show that a substantial part of the recent negative global mean and tropical mean OLR ARCs results from the contribution of OLR anomalies contained within OLR Region 1 to the overall statistics.

Water vapor and cloud cover anomalies in the relatively small OLR Region 2 also contribute significantly to the recent decreases in global and tropical OLR. One-third of this region is in the tropics and the remaining two-thirds is in the subtropics. As shown in Table 2, both OLR data sets show that otherwise global and tropical mean ARCs, computed after exclusion of OLR anomalies in both OLR Regions 1 and 2, are essentially zero. Table 2 shows that ENCs of global and tropical mean OLR are also substantially reduced when anomalies in OLR Regions 1 and 2 are excluded from the calculations.

8. Summary

The first part of this paper compared September 2002 through June 2011 anomaly time series of OLR and OLR_{CLR} data records, determined from CERES observations as generated by the CERES Science Team, and from AIRS observations as generated by the AIRS Science Team. Excellent agreement was found between the CERES and AIRS OLR anomaly time series down to the 1 degree latitude by 1 degree longitude spatial scale. CERES and AIRS data records both show that global mean and tropical mean OLR have decreased over the time period under study, and more significantly, that both global and tropical mean OLR anomaly time series are highly positively correlated with El Niño/La Niña variability as expressed by an El Niño Index.

The paper then used anomaly time series of surface skin temperature, mid-tropospheric water vapor, and cloud amounts derived from analysis of AIRS sounder data over this time period to explain why global and tropical mean OLR anomaly time series are positively correlated with the El Niño Index, which like global and tropical mean OLR, has decreased on the average over this time period as a result of phases of El Niño/La Niña oscillations.

The AIRS results shown in this paper were based on products derived using the AIRS Science Team Version-5 retrieval algorithm. The AIRS Version-6 retrieval algorithm is expected to become operational in mid-2012, and will be used to analyze all future AIRS observations as well as reanalyze all previous AIRS observations. As shown in this paper, AIRS Version-6 OLR and OLR_{CLR} data records should be much closer in the mean to those of CERES. AIRS Version-6 data records will also include monthly mean values of the spectral components of OLR averaged over each of the 16 contiguous spectral bands used in the computation of OLR in Version-6. Anomaly time series of OLR computed only over each of these spectral intervals, and the spatial distribution of their Average Rates of Change and El Niño anomaly correlations, will provide important additional information to help understand the effect of El Niño/La Niña oscillations on OLR.

The results shown in this paper should not be taken in any way as to be indicative of how OLR will change in the future. The EOS satellites carrying AIRS and CERES are expected to last about 20 years. Having a 20 year time series of overlapping AIRS and CERES OLR data records would be a very useful first step towards monitoring and understanding long term variability of OLR. Continuation of

AIRS class and CERES class instrumentation beyond the EOS era will be needed to fully monitor and understand longer term changes in OLR.

References:

Allan, R. P., and M. A. Ringer, 2003: Inconsistencies between satellite estimates of longwave cloud forcing and dynamical fields from reanalyzes. *Geophys. Res. Lett.*, **30,** 4.

Barkstrom, B., E. Harrison, G. Smith, R. Green, J. Kibler, R. Cess, the ERBE Science Team,1989: Earth Radiation Budget (ERBE) Archival and April 1985 Results. *Bulletin of the American Meteorological Society*, **70**, 1254-1262.

Barlow, M., M. Wheeler, B. Lyon, and H. Cullen, 2005: Modulation of Daily Precipitation over Southwest Asia by the Madden-Julian Oscillation. *Mon. Weather Rev.*, **133,** 3579-3594.

Brown, J. R., S. B. Power, F. P. Delage, R. A. Colman, A. F. Moise, B. F. Murphy, 2011: Evaluation of the South Pacific Convergence Zone in IPCC AR4 Climate Model Simulations of the Twentieth Century. *J. Climate*, **24**, 1565-1582. doi:10.1175/2010JCLI3942.1.

Chiodi, A. M., and D. E. Harrison, 2010: Characterizing Warm-ENSO Variability in the Equatorial Pacific: An OLR Perspective. *J. Clim.*, **23,** 2428-2439.

Chu, P. S., and J. B. Wang, 1997: Recent Climate Change in the Tropical Western Pacific and Indian Ocean Regions as Detected by Outgoing Longwave Radiation Records. *J. Clim.*, **10,** 636-646.

Chung, E. S., D. Yeomans, and B. J. Soden, 2010: An assessment of climate feedback processes using satellite observations of clear-sky OLR. *Geophys. Res. Lett.*, **37,** 7.

Clement, A. C., B. Soden, 2005: The Sensitivity of the Tropical-Mean Radiation Budget. *J. Climate*, **18**, 3189-3203. doi: 10.1175/JCLI3456.1.

Davis, R., M. Molloy, 2012: Global Cloud Height Fluctuations Measured by MISR on Terra from 2000 to 2010. *Geophys. Res. Lett.*, **39**, L03701, doi:10.1029/2011GL050506.

Dessler, A. E., Z. Zhang, and P. Yang, 2008: Water-vapor Climate Feedback Inferred from Climate Fluctuations, 2003-2008. *Geophys. Res. Lett.*, **35**, L20704, doi: 10.1029/2008GL035333.

Dessler, A. E., 2010: A Determination of the Cloud Feedback from Climate Variations over the Past Decade. *Science*, **330**, 1523-1527. doi: *10.1126/science.1192546*

Doelling, D. R., N. G. Loeb, D. F. Keyes, M. K. Nordeen, D. Morstad, B. A. Wielicki, D. F. Young, and M. Sun, 2012: Geostationary Enhanced Temporal Interpolation for CERES Flux Products. J. *Appl. Meteor. & Climate* (in preparation).

Draper, N. and H. Smith, 1981: Applied Regression Analysis, Second Edition. *Wiley*, ISBN 047102995-5.

Fasullo, J. T., and K. E. Trenberth, 2008: The Annual Cycle of the Energy Budget. Part II: Meridional Structures and Poleward Transports. *J. Clim.*, **21,** 2313-2325.

Folland, C. K., J. A. Renwick, M. J. Salinger, and A. B. Mullan, 2002: Relative influences of the Interdecadal Pacific Oscillation and ENSO on the South Pacific Convergence Zone. *Geophys. Res. Lett*., **29**, 13 doi:10.1029/2001GL014201.

Gruber, A., R. Ellingson, P. Ardanuy, M. Weiss, S. K. Yang, and S. N. Oh, 1994: A Comparison of ERBE and AVHRR Longwave Flux Estimates. *Bulletin of the American Meteorological Society*, **75,** 2115-2130.

Jones, C., L. M. V. Carvalho, R. W. Higgins, D. E. Waliser, and J. K. E. Schemm, 2004: Climatology of Tropical Intraseasonal Convective Anomalies: 1979-2002. *J. Clim.*, **17,** 523-539.

Kidson, J. W., M. J. Revell, B. Bhaskaran, A. B. Mullan, and J. A. Renwick, 2002: Convection Patterns in the Tropical Pacific and Their Influence on the Atmospheric Circulation at Higher Latitudes. *J. Clim.*, **15,** 137-159.

Kiladis, G. N., K. H. Straub, and P. T. Haertel, 2005: Zonal and Vertical Structure of the Madden-Julian Oscillation. *Journal of the Atmospheric Sciences*, **62,** 2790-2809.

Kyle, H. L., A. Arking, J. R. Hickey, P. E. Ardanuy, H. Jacobowitz, H. Jacobowitz, L. L. Stowe, G. G. Campbell, T. Vonder Haar, F. B. House, R. Maschhoff, and G. L. Smith, 1993: The Nimbus Earth Radiation Budget (ERB) Experiment: 1975-1992. *Bull. Am. Meteorol. Soc*., **74**, 815-830.

Loeb, N. G., S. Kato, K. Loukachine, and N. Manalo-Smith, 2005: Angular Distribution Models for Top-of-Atmosphere Radiative Flux Estimation from the Clouds and the Earth's Radiant Energy System Instrument on the *Terra* Satellite. Part 1: Methodology. *J. Atmos. Ocean. Tech*., **22**(4), 338-351.doi:10.1175/JTECH1712.1.

Loeb, N. G., S. Kato, W. Su, T. Wong, F. Rose, D. Doelling, J. Norris, 2012a: Advances in Understanding Top-of-Atmosphere Radiation Variability from Satellite Observations. *Surveys in Geophysics*, doi:10.1007/S10712-012-9175-1.

Loeb, N. G., J. M. Lyman, G. C. Johnson, R. P. Allan, D. R. Doelling, 2012b: Observed Changes in Top-of-the-atmosphere Radiation and Upper-ocean Heating Consistent within Uncertainty. *Nature Geoscience*, doi:10.1038/NGE01375 and supplementary information.

McClatchey, R. A., R. W. Fenn, J. E. A. Selby, F. E. Volz, and J. S. Garing, 1972: Optical Properties of the Atmosphere (Third Edition). *Environ. Res. Papers*, **411**, AFCRL, Bedford, MA, 108 pp.

Mehta, A. V. and J. Susskind, 1999a: Outgoing Longwave Radiation from the TOVS Pathfinder Path A Data Set. *J. of Geophys. Res*., **104**, 12193-12212.

Mehta, A. V. and J. Susskind, 1999b: Longwave Radiative Flux Calculations in the TOVS Pathfinder Path A Data Set. *NASA Tech. Rep., GSFC/CR-1999-208643*.
Proc. SPIE International Symp. Infrared Spaceborne Remote Sensing and Instrumentation XVII, San Diego, CA, August 2009.

Minnis, P., Q. Z. Trepte, S. Sun-Mack, Y. Chen, D. R. Doelling, et al., 2008: Cloud Detection in Non-polar Regions for CERES Using TRMM VIRS and Terra and Aqua MODIS Data. *IEEE Trans. Geosci. Remote Sens*., **46**, 3857-3884.

Minnis, P., S. Sun-Mack, D. F. Young, P. W. Heck, D. P. Garber, et al., 2011: CERES Edition-2 Cloud Property Retrievals Using TRMM VIRS and Terra and Aqua MODIS data. Part 1: Algorithms. *IEEE Trans. Geosci. Remote Sens*. (in press).

Power, S. B., and I. N. Smith, 2007: Weakening of the Walker Circulation and apparent dominance of El Niño both reach record levels, but has ENSO really changed?, *Geophys. Res. Lett*., **34**, L18702, doi:10.1029/2007GL030854.

Soden, B. J., and I. M. Held, 2006: An Assessment of Climate Feedbacks in Coupled Ocean–Atmosphere Models. *J. Clim.*, **19,** 3354-3360.

Soden, B. J., I. M. Held, R. Colman, K. M. Shell, J. F. Kiehl, C. A. Shields, 2008: Quantifying Climate Feedbacks Using Radiative Kernels. *J. Clim*., **21**, 3504-3520.

Susskind, J. and J. E. Searl, 1978: Synthetic Atmospheric Transmittance Spectra Near 15 μm and 4.3 μm. *J. Quant. Spectr. Rad. Trans*., **19**, 195-215.

Susskind, J., P. Piraino, L. Rokke, L. Iredell, and A. V. Mehta, 1997: Characteristics of the TOVS Pathfinder Path A Data Set. *Bull. of Amer. Meteorol. Soc*., **78**, 1449-1472.

Susskind, J., C.D. Barnet, J.M. Blaisdell, 2003: Retrieval of atmospheric and surface parameters from AIRS/AMSU/HSB data in the presence of clouds. IEEE Transactions on Geoscience and Remote Sensing, Issue 2, **41**, doi: 10.1109/TGRS.2002.808236, 390-409.

Susskind, J., J. Blaisdell, and L. Iredell, 2009: Improved Determination of Surface and Atmospheric Temperatures Using Only Shortwave AIRS Channels. *Proc. SPIE International Symp. Infrared Spaceborne Remote Sensing and Instrumentation XVII*, San Diego, CA, August 2009.

Susskind, J., J. M. Blaisdell, L. Iredell, and F. Keita, 2011a: Improved Temperature Sounding and Quality Control Methodology Using AIRS/AMSU Data: The AIRS Science Team Version 5 Retrieval Algorithm. Geoscience and Remote Sensing, IEEE Transactions on Geoscience and Remote Sensing, Issue: 99 Digital Object Identifier: 10.1109/TGRS.2010.2070508, 1-25.

Susskind, J., J. Blaisdell, and L. Iredell, 2011b: Improved Surface and Tropospheric Temperature Determined Using Only Shortwave Channels: The AIRS Science Team Version-6 Retrieval Algorithm. *Proc. SPIE Optics and Photonics*, Paper #8153-5, San Diego, CA, August 2011.

Trenberth, E. T., J. T. Fasullo, C. O'Dell, and T. Wong, 2010: Relationships between tropical sea surface temperature and top-of-atmosphere radiation. *Geophys. Res. Lett.*, **37**, L03702, doi:10.1029/2009GL042314.

Wielicki, B. A., B. R. Barkstrom, E. F. Harrison, R. B. Lee III, G. L. Smith, and J. E. Cooper, 1996: Clouds and the Earth's Radiant Energy System (CERES): An Earth Observing System Experiment. *Bull. Amer. Meteor. Soc*., **77**, 853-868.

Wong, T., B. A. Wielicki, R. B. Lee, III, G. L. Smith, K. A. Bush, J. K. Willis, 2006: Reexamination of the Observed Decadal Variability of the Earth Radiation Budget Using Altitude-Corrected ERBE/ERBS Nonscanner WFOV Data. *J. Climate*, **19**, 4028-4040.

Zhou, Y. P., K.-M. Xu, Y. C. Sud, and A. K. Betts, 2011: Recent Trends of the Tropical Hydrological Cycle Inferred from Global Precipitation Climatology Project and International Satellite Cloud Climatology Project Data. *J. Geophys. Res*., **116**, D09101, doi: 10.1029/2010JD015197.

Table 1a. OLR Anomaly Time Series Comparison
September 2002 through June 2011

Data Set	Global	Tropical
AIRS ARC ($W/m^2/yr$)	−0.094 ± 0.026	−0.183 ± 0.070
CERES Terra ARC ($W/m^2/yr$)	−0.059 ± 0.022	−0.154 ± 0.066
AIRS Minus CERES STD (W/m^2)	0.136	0.155
AIRS/CERES Correlation	0.955	0.991

Global and Tropical mean statistical comparisons of AIRS and CERES OLR anomaly time series for the period September 2002 through June 2011. Shown are the Average Rates of Change, the standard deviations between the anomaly time series, and the temporal correlations of the anomaly time series.

Table 1b. OLR_{CLR} Anomaly Time Series Comparison
September 2002 through June 2011

Data Set	Global	Tropical
AIRS ARC ($W/m^2/yr$)	−0.021 ± 0.020	−0.072 ± 0.042
CERES Terra ARC ($W/m^2/yr$)	−0.089 ± 0.020	−0.144 ± 0.044
AIRS Minus CERES STD (W/m^2)	0.222	0.247
AIRS/CERES Correlation	0.772	0.936

Global and Tropical mean statistical comparisons of AIRS and CERES OLR_{CLR} anomaly time series for the period September 2002 through June 2011. Shown are the Average Rates of Change, the standard deviations between the anomaly time series, and the temporal correlations of the anomaly time series.

Table 1c. Correlations between Global and Tropical Mean OLR and OLR_{CLR} Anomaly Time Series, September 2002 through June 2011

AIRS and CERES

	Global OLR	Tropical OLR	Global OLR_{CLR}	Tropical OLR_{CLR}	El Niño Index
Global OLR	**---**	**0.705**	**0.720**	**0.608**	**0.587**
Tropical OLR	0.646	**---**	**0.616**	**0.871**	**0.830**
Global OLR_{CLR}	0.797	0.696	**---**	**0.799**	**0.502**
Tropical OLR_{CLR}	0.663	0.928	0.827	**---**	**0.730**
El Niño Index	0.523	0.813	0.618	0.808	**---**

Temporal correlations of AIRS and CERES OLR and OLR_{CLR} global and tropical anomaly time series. Correlations using AIRS data records are shown above the diagonal in bold and those using CERES data are shown beneath the diagonal.

Table 2. Area Mean Statistics for AIRS and CERES OLR
September 2002 through June 2011

	AIRS		CERES	
Spatial Area	OLR ARC ($W/m^2/yr$)	OLR ENC	OLR ARC ($W/m^2/yr$)	OLR ENC
Region1	-0.631 ± 0.158	0.767	-0.611 ± 0.154	0.761
Region 2	-1.660 ± 0.348	0.818	-1.534 ± 0.348	0.825
Global without Region 1	-0.044 ± 0.020	0.256	-0.011 ± 0.019	0.039
Tropical without Region 1	-0.037 ± 0.048	0.599	-0.011 ± 0.047	0.511
Global without Region 1&2	-0.011 ± 0.021	-0.098	0.021 ± 0.020	-0.331
Tropical without Region1&2	-0.005 ± 0.045	0.468	0.022 ± 0.044	0.362

Area mean Average Rates of Change of AIRS and CERES OLR anomaly time series, and the correlation between the OLR anomaly time series and the EL Niño Index, computed over the period September 2002 through June 2011 over different spatial domains.

Figure and Table Captions

Figure 1

a) Monthly mean global mean time series values of AIRS Version-5 and CERES Terra Edition-2.6 OLR and OLR_{CLR} for the period September 2002 through June 2011. Monthly mean values of AIRS Version-6 OLR and OLR_{CLR} products are also shown for April 2003 and April 2011. b) Global monthly mean differences of values shown for Figure 1a. The green and red horizontal lines show the average values of the differences between AIRS and CERES OLR and AIRS and CERES OLR_{CLR} respectively.

Figure 2

Monthly mean global mean AIRS and CERES Terra OLR anomaly time series and their anomaly differences for the period September 2002 through June 2011. a) Global mean OLR anomalies. b) Tropical mean (20°N to 20°S) anomalies, as well as the El Niño Index multiplied by 1.5. c) As in a) but for $OLR_{CLR,}$ and d) as in b) but for OLR_{CLR}.

Figure 3

Spatial 1° latitude by 1° longitude distribution of OLR ARCs over the time period September 2002 through June 2011. The NOAA Niña-4 region is outlined in gray and OLR Regions 1 and 2 are outlined in black in this and most subsequent figures showing spatial distributions of ARCs of different parameters. a) AIRS OLR ARCs, b) CERES OLR ARCs, c) AIRS minus CERES OLR ARCs, and d) AIRS minus CERES OLR_{CLR} ARCs.

Figure 4

Spatial 1° latitude by 1° longitude distribution of OLR correlations over the time period September 2002 through June 2011: a) AIRS OLR ENCs, b) CERES OLR ENCs, c) AIRS minus CERES OLR ENCs, d) AIRS and CERES OLR anomaly correlations.

Figure 5

Hovmöller diagram for time series of monthly mean anomalies (vertical scale) integrated over the latitude range 5°N through 5°S in each 1° longitude bin (horizontal scale) for the period September 2002 through June 2011. The longitudinal domain of OLR Region 1 is indicated by the black vertical lines in this and most subsequent Hovmöller diagrams. a) AIRS OLR, b) CERES OLR, c) the difference between AIRS and CERES OLR anomalies.

Figure 6

Spatial distribution of ARCs and ENCs of AIRS retrieved geophysical parameters for the period September 2002 through June 2011. a) ARCs of Surface Skin Temperature (K/yr). b) ENCs of Surface Skin Temperature. c) ENCs of q_{500}. d) ENCs of $\alpha\varepsilon$.

Figure 7

Hovmöller diagrams of AIRS retrieved products. a) T_{skin}. The longitudinal domain of the NOAA Niño-4 region is encompassed by the gray vertical lines b) q_{500}. The longitudinal domain of OLR Region 1 is encompassed by the thick black vertical lines. c) as in b) but for $\alpha\varepsilon$.

Table 1a

Global and Tropical statistical comparisons of OLR anomaly time series for the period September 2002 through June 2011 for AIRS and CERES Terra OLR. Shown are the Average Rates of Change, the standard deviations between the anomaly time series, and the temporal correlations of the anomaly time series.

Table 1b

Global and Tropical statistical comparisons of OLR_{CLR} anomaly time series for the period September 2002 through June 2011 for AIRS and CERES Terra OLR_{CLR}. Shown are the Average Rates of Change, the standard deviations between the anomaly time series, and the temporal correlations of the anomaly time series.

Table 1c

Temporal correlations of AIRS and CERES OLR and OLR_{CLR} global and tropical anomaly time series. Correlations using AIRS data records are shown above the diagonal in bold and those using CERES data are shown beneath the diagonal.

Table 2

Area mean Average Rates of Change of AIRS and CERES OLR anomaly time series, and the correlation between the OLR anomaly time series and the El Niño Index, computed over the period September 2002 through June 2011 over different spatial domains.

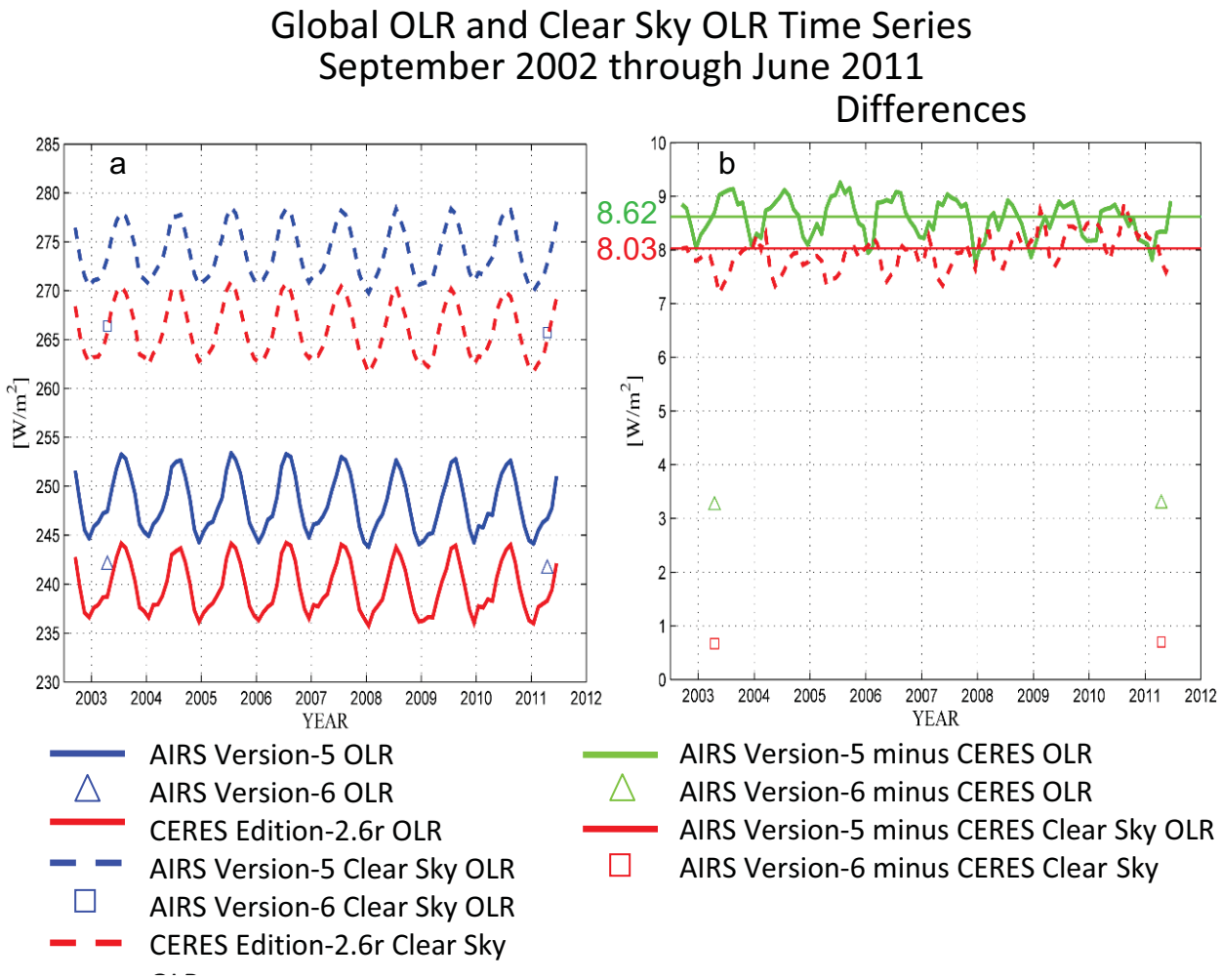
Global OLR and Clear Sky OLR Time Series
September 2002 through June 2011
Differences
a
b
8.62
8.03
[W/m2]
YEAR
AIRS Version-5 OLR
AIRS Version-6 OLR
CERES Edition-2.6r OLR
AIRS Version-5 Clear Sky OLR
AIRS Version-6 Clear Sky OLR
CERES Edition-2.6r Clear Sky
AIRS Version-5 minus CERES OLR
AIRS Version-6 minus CERES OLR
AIRS Version-5 minus CERES Clear Sky OLR
AIRS Version-6 minus CERES Clear Sky

Figure 1

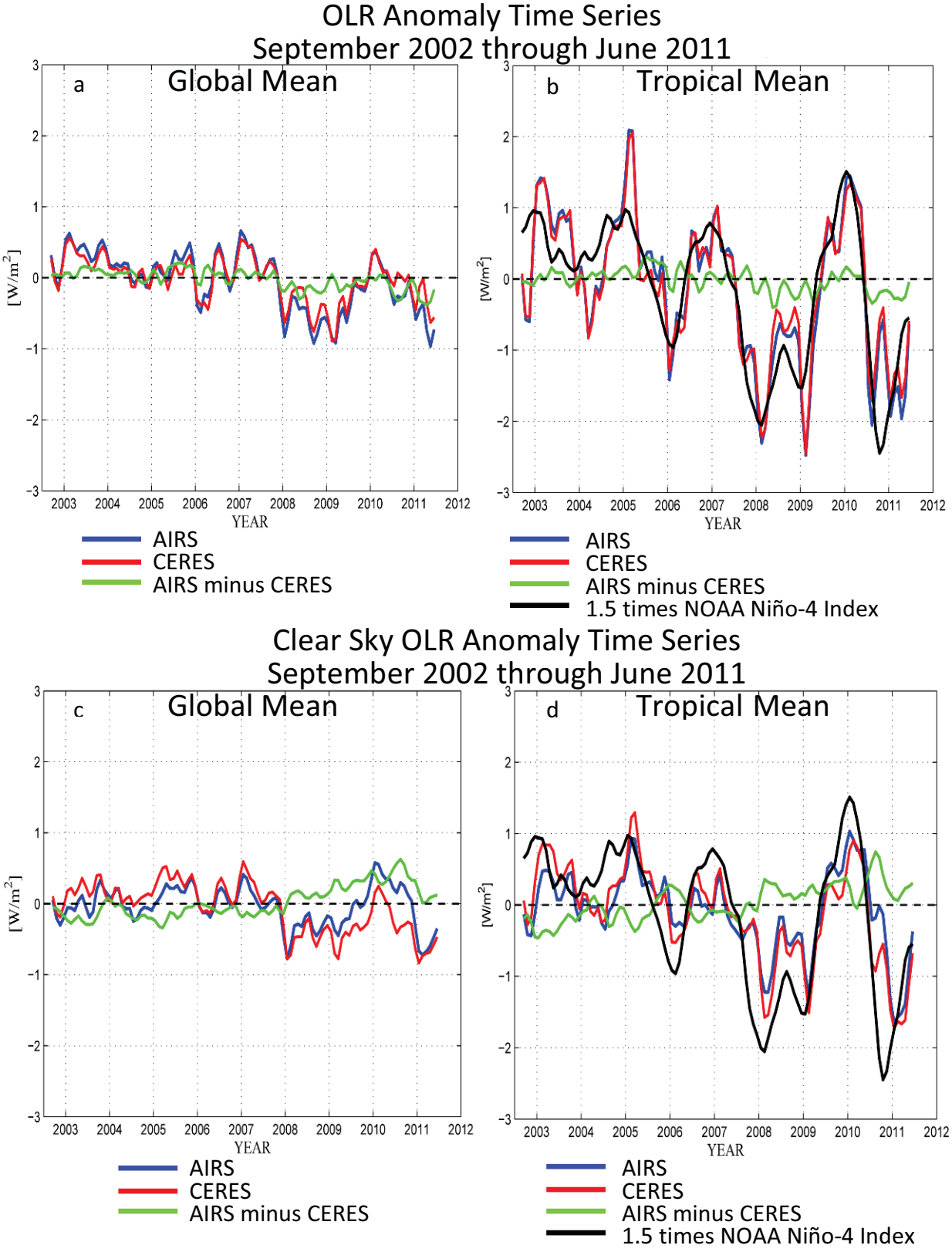
OLR Anomaly Time Series
September 2002 through June 2011
a
Global Mean
b
Tropical Mean
[W/m2]
YEAR
AIRS
CERES
AIRS minus CERES
1.5 times NOAA Niño-4 Index
Clear Sky OLR Anomaly Time Series
September 2002 through June 2011
c
Global Mean
d
Tropical Mean

Figure 2

Average Rates of Change (ARCs)
September 2002 through June 2011

a) AIRS OLR

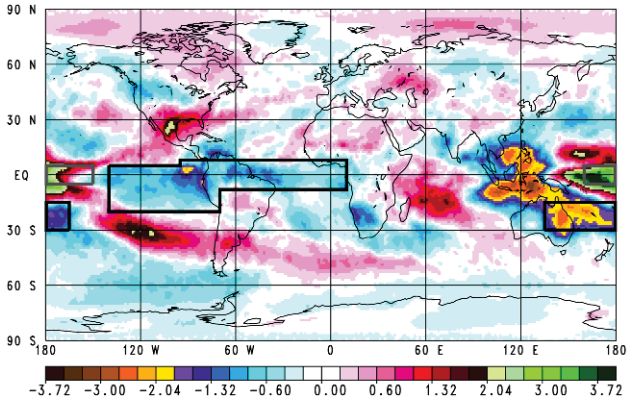

Global Mean=-0.094 STD= 0.82

b) CERES OLR

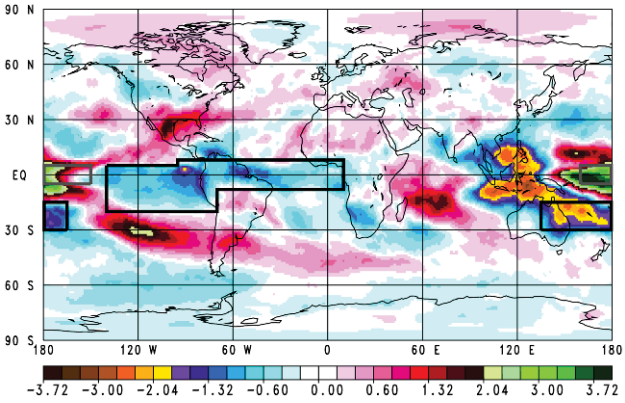

Global Mean=-0.059 STD=0.82

c) AIRS minus CERES OLR

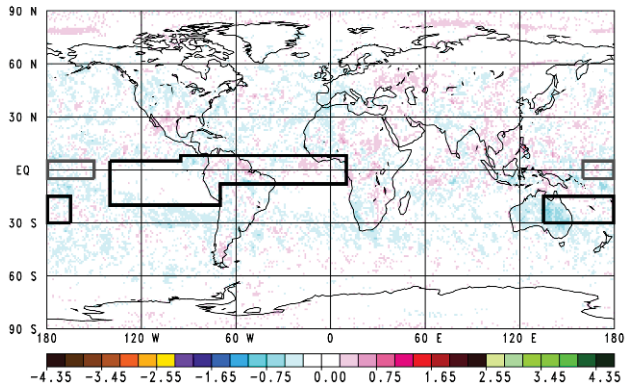

Global Mean=-0.035 STD=0.15 Corr=0.98

d) AIRS minus CERES Clear Sky OLR

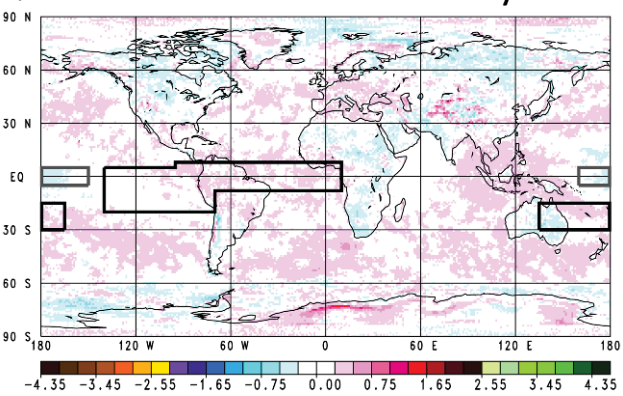

Global Mean=0.068 STD=0.16 Corr=0.82

Figure 3

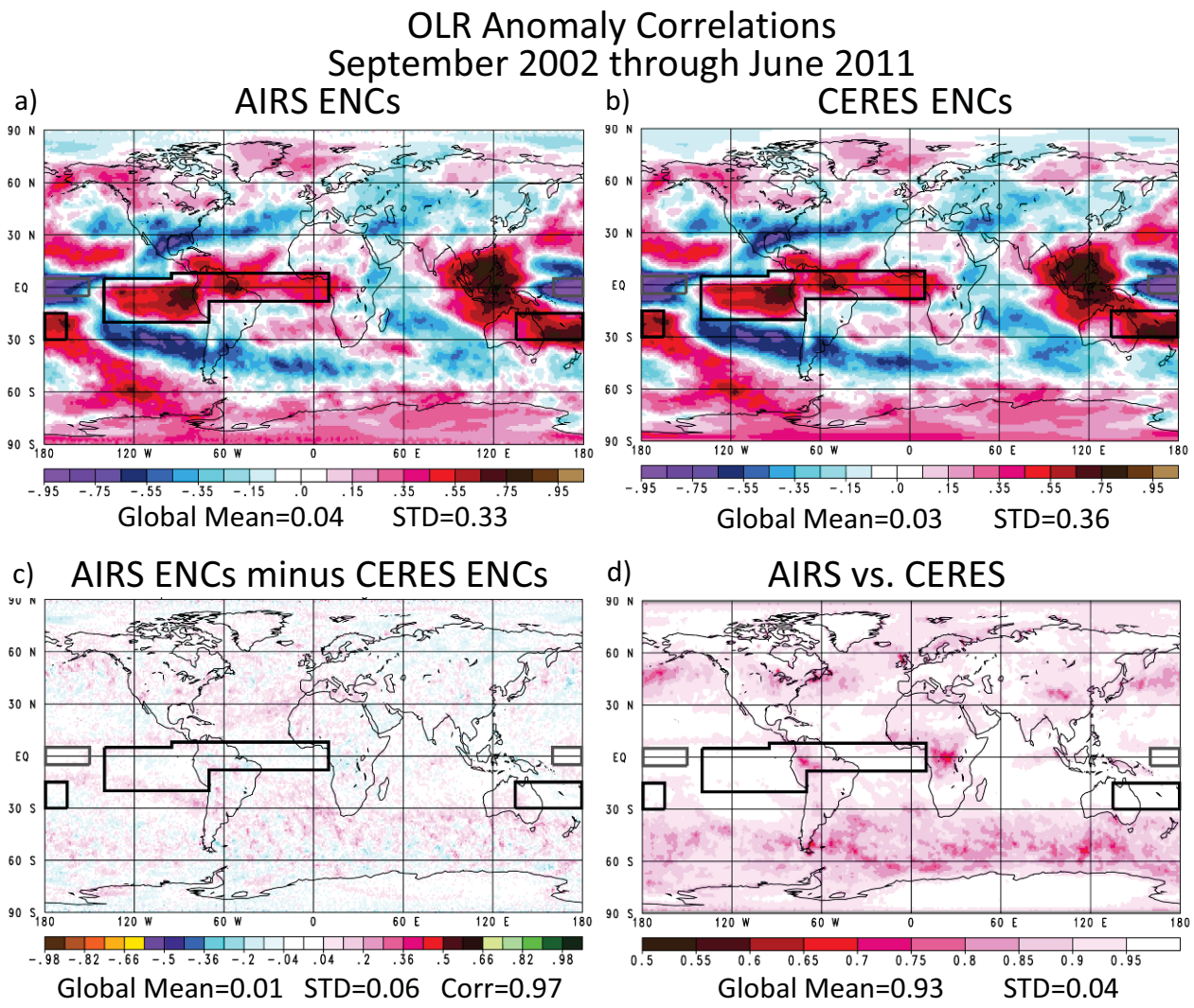
OLR Anomaly Correlations
September 2002 through June 2011
a)
AIRS ENCs
b)
CERES ENCs
Global Mean=0.04 STD=0.33
Global Mean=0.03 STD=0.36
c)
AIRS ENCs minus CERES ENCs
d)
AIRS vs. CERES
Global Mean=0.01 STD=0.06 Corr=0.97
Global Mean=0.93 STD=0.04

Figure 4

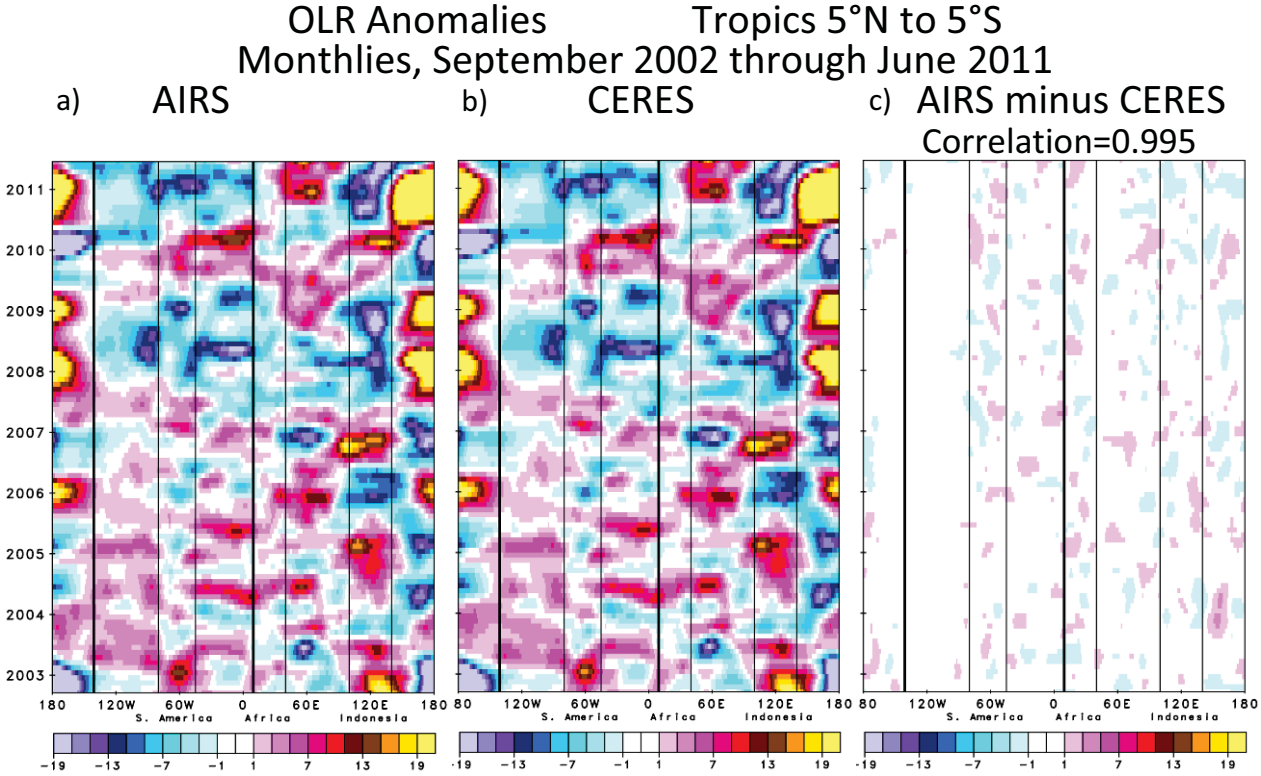
OLR Anomalies Tropics 5°N to 5°S
Monthlies, September 2002 through June 2011
a) AIRS
b) CERES
c) AIRS minus CERES
Correlation=0.995
2011
2010
2009
2008
2007
2006
2005
2004
2003
180 120W 60W 0 60E 120E 180
S. America Africa Indonesia
-19 -13 -7 -1 1 7 13 19

Figure 5

AIRS Products September 2002 through June 2011

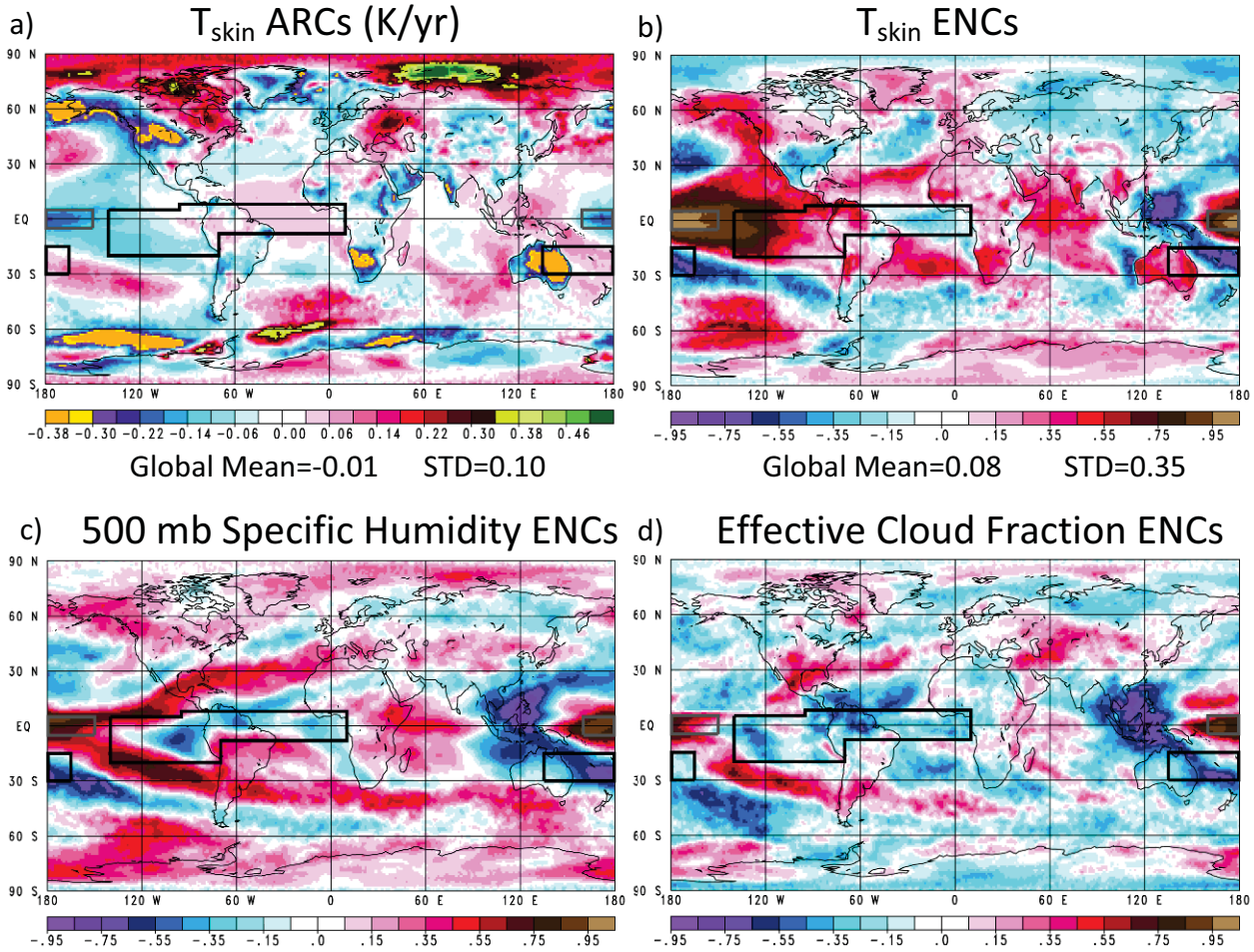

Figure 6

AIRS Anomalies Tropics 5°N to 5°S
Monthlies, September 2002 through June 2011

a) Skin Temperature (K) b) 500 mb Specific Humidity (%) c) Cloud Fraction (%)

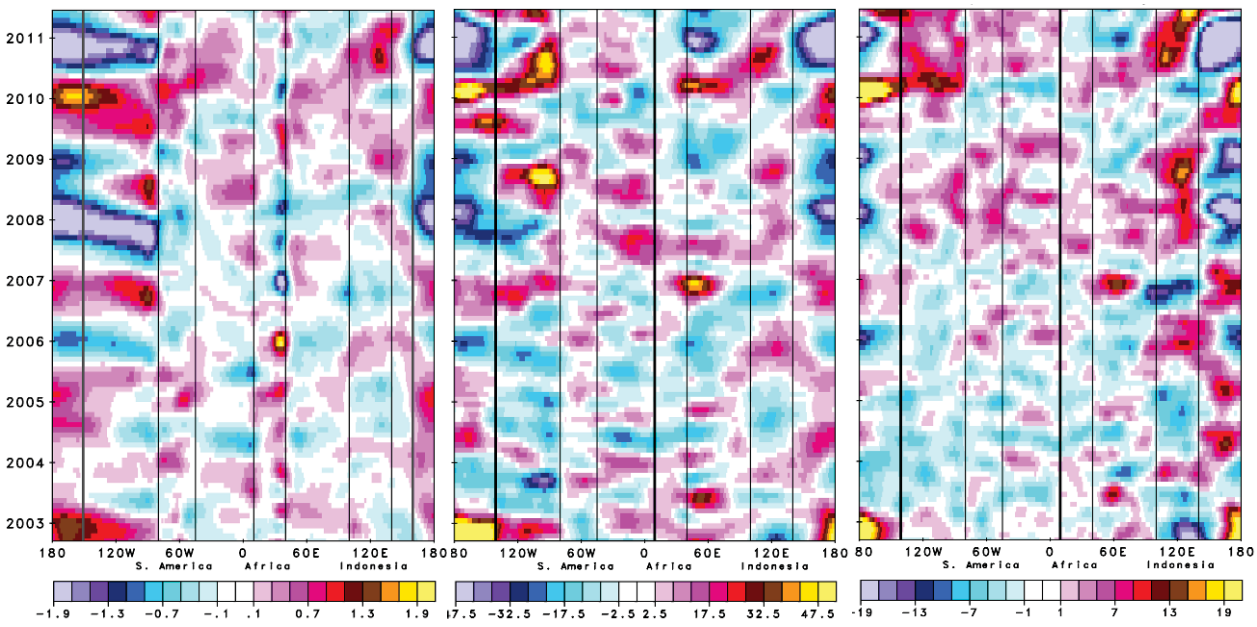

Figure 7